J|A|C|S
ARTICLES
Published on Web 12/04/2002

Syntheses and Structural Characterizations of *endo*-η^1-, *exo*-η^1-, η^4-, η^5-, and η^6-Metallaphosphamonocarbaborane Complexes Derived from a Versatile New Polyborane Ligand: *exo*-6-R-*arachno*-6,7-PCB_8H_{12}

Daniel E. Kadlecek,[1] Alexandra M. Shedlow,[1] Sang Ook Kang,[2] Patrick J. Carroll,[1] and Larry G. Sneddon*,[1]

Contribution from the Department of Chemistry, University of Pennsylvania, Philadelphia, Pennsylvania 19104-6323, and Korea University, Seochang 208 Jochiwon, Choongnam, Korea, 339−800

Received July 9, 2002

Abstract: Deprotonation of the phosphamonocarbaborane, *exo*-6-R-*arachno*-6,7-PCB_8H_{12} (R = Ph **1a** or Me **1b**), yields *exo*-6-R-*arachno*-6,7-$PCB_8H_{11}^-$, which when reacted with appropriate transition-metal reagents affords new metallaphosphamonocarbaborane complexes in which the metals adopt *endo*-η^1, *exo*-η^1, η^4, η^5, or η^6 coordination geometries bonded to the formal R-*arachno*-$PCB_8H_{11}^-$, R-*arachno*-$PCB_8H_{10}^{2-}$, R-*arachno*-$PCB_8H_9^{3-}$, or R-*nido*-$PCB_8H_9^-$ ligands. The reaction of *exo*-6-(C_6H_5)-*arachno*-6,7-$PCB_8H_{11}^-$ (**1a**$^-$) with $Mn(CO)_5Br$ generated the η^1-sigma product *exo*-6-[$Mn(CO)_5$]-*endo*-6-(C_6H_5)-*arachno*-6,7-PCB_8H_{11} (**2**) having the [$Mn(CO)_5$] fragment in the thermodynamically favored exo position at the P6 cage atom. On the other hand, reaction of **1a**$^-$ with (η^5-C_5H_5)Fe$(CO)_2$I resulted in the formation of two products, an η^1-sigma complex *endo*-6-[(η^5-C_5H_5)Fe$(CO)_2$]-*exo*-6-(C_6H_5)-*arachno*-6,7-PCB_8H_{11} (**3**) having the (η^5-C_5H_5)Fe$(CO)_2$ fragment attached at the *endo*-P6 position and an η^6-*closo* complex, 1-(η^5-C_5H_5)-2-(C_6H_5)-*closo*-1,2,3-$FePCB_8H_9$ (**4a**). Rearrangement of the *endo*-compound **3** to its *exo*-isomer **5** was observed upon photolysis of **3**. Synthesis of the methyl analogue of **4a**, 1-(η^5-C_5H_5)-2-CH_3-*closo*-1,2,3-$FePCB_8H_9$ (**4b**), along with a double-insertion product, 1-CH_3-2,3-(η^5-C_5H_5)$_2$-2,3,1,7-$Fe_2PCB_8H_9$ (**6**), containing two iron atoms η^5-coordinated to a formal R-*arachno*-$PCB_8H_9^{3-}$, was achieved by reaction of *exo*-6-CH_3-*arachno*-6,7-$PCB_8H_{11}^-$ (**1b**$^-$) with $FeCl_2$ and $Na^+C_5H_5^-$. Complexes **4a** and **4b** can be considered ferrocene analogues, in which an Fe(II) is sandwiched between $C_5H_5^-$ and 6-R-*nido*-6,9-$PCB_8H_9^-$ anions. Reaction of *exo*-6-(C_6H_5)-*arachno*-6,7-$PCB_8H_{11}^-$ (**1a**$^-$) with *cis*-dichlorobis(triphenylphosphine)platinum (II) afforded two compounds, an η^1-sigma complex with the metal fragment again in the *endo*-P6 position, *endo*-6-[*cis*-(Ph_3P)$_2$PtCl]-*exo*-6-(C_6H_5)-*arachno*-6,7-PCB_8H_{11} (**7**) and an η^4-complex, 7-(C_6H_5)-11-(Ph_3P)$_2$-*nido*-11,7,8-$PtPCB_8H_{10}$ (**8**) containing the formal R-*arachno*-$PCB_8H_{10}^{2-}$ anion. The structures of compounds **2**, **3**, **4a**, **4b**, **6**, **7**, and **8** were crystallographically confirmed.

Introduction

The structure that was confirmed[3] using DFT/GIAO (B3LYP/6-311G*) methods for the *exo*-6-R-*arachno*-6,7-PCB_8H_{12} phosphamonocarbaborane **1** is shown in Figure 1. In agreement with its 26 skeletal-electron count, the compound adopts a 10-vertex arachno geometry on the basis of an icosahedron missing two vertexes. The phosphorus and carbon atoms are in adjacent positions, 6 and 7, on the puckered six-membered open face, with the P6 phosphorus atom having an exopolyhedral substituent (R = Ph, **1a**, and R = Me, **1b**) and an *endo*-hydrogen. The two bridge protons span the B8−B9 and B9−B10 edges. Since cluster *endo*- and bridging-hydrogens are normally acidic, it should be possible to derive, as illustrated in Figure 2, a variety of anions by deprotonation of **1**. In the preceding paper,[3] it was shown that mono-deprotonation results in the removal of the P6 *endo*-hydrogen to produce the 6-R-*arachno*-6,7-$PCB_8H_{11}^-$ monoanion. Deprotonation of the bridging hydrogens by the addition of two and three equivalents of base could, in principle,

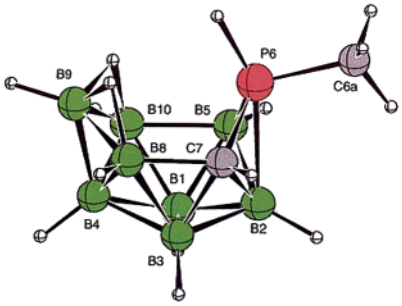

Figure 1. Structure of the phosphamonocarbadecaborane, *exo*-6-R-*arachno*-6,7-PBC_8H_{12} (**1**).

* Address correspondence to this author. E-mail: lsneddon@sasupenn.edu.
(1) University of Pennsylvania.
(2) Korea University.
(3) Shedlow, A. M.; Kadlecek, D. E.; Rathmill, S.; Clapper, J. C.; Carroll, P.; Sneddon, L. G. *J. Am. Chem. Soc.* 2002, *124*, 200−211.

10.1021/ja020945b CCC: $25.00

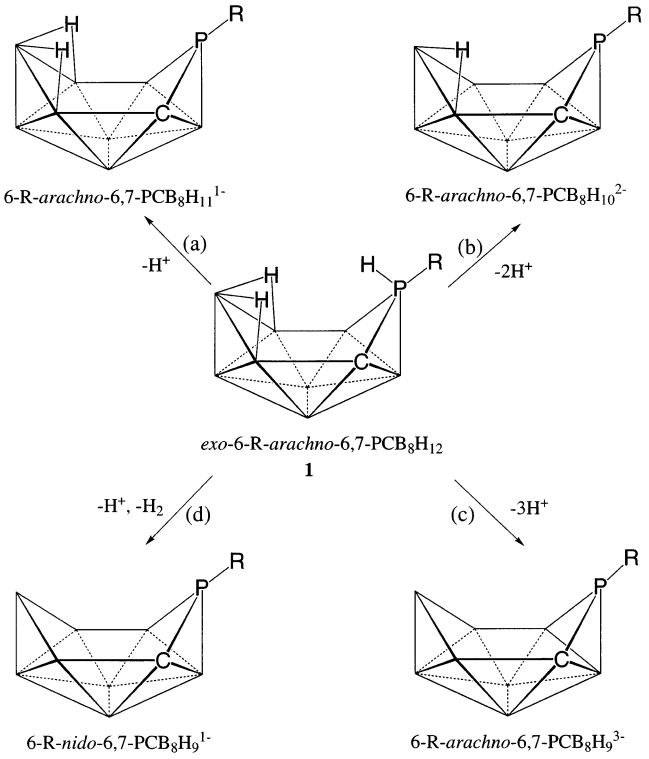

Figure 2. The range of possible anions derived from *exo*-6-R-*arachno*-6,7-PBC$_8$H$_{12}$ (**1**).

generate the arachno di- and trianions, 6-R-*arachno*-6,7-PCB$_8$H$_{10}^{2-}$ and 6-R-*arachno*-6,7-PCB$_8$H$_9^{3-}$, respectively. Formation of the nido monoanion 6-R-*nido*-6,7-PCB$_8$H$_9^-$ could also be possible by mono-deprotonation of **1** accompanied by loss of molecular hydrogen, as given in path d in the figure. Such a 6-R-*nido*-6,7-PCB$_8$H$_9^-$ monoanion would, in fact, be an isomer of the 6-R-*nido*-6,9-PCB$_8$H$_9^-$ anion reported in the preceding paper.[3] In this paper, we describe the syntheses and structural characterization of a wide variety of new types of metallaphosphamonocarbaborane complexes formally derived from these four anions in which the metals adopt an unprecedented array of coordination geometries, including *endo*-η^1, *exo*-η^1, η^4, η^5, and η^6 bonding configurations.

Experimental Section

All manipulations were carried out using standard high-vacuum or inert-atmosphere techniques as described by Shriver.[4]

Materials. Proton Sponge (1,8-bis(dimethylamino)naphthalene, PS), (η^5-C$_5$H$_5$)Fe(CO)$_2$I and 2.0 M sodium cyclopentadienide (Na$^+$C$_5$H$_5^-$) in THF were purchased from Aldrich and used as received. Oil dispersed NaH and KH were purchased from Aldrich, washed with dry hexanes under a N_2 atmosphere, and then dried under vacuum. $FeCl_2$ was dried for 15 h at 120 °C in vacuo and stored under a N_2 atmosphere until use. Mn(CO)$_5$Br was purchased from Strem and used as received. *cis*-Dichlorobis(triphenylphosphine)platinum (II) was purchased from Pressure Chemical and used as received. Tetrahydrofuran and dimethoxyethane (DME) were dried over sodium/benzophenone ketyl and distilled prior to use. Hexanes, toluene, and dichloromethane were purchased from Fisher and used as received. The phosphamonocarbaborane *exo*-6-R-*arachno*-6,7-PCB$_8$H$_{12}$ (**1**) was prepared according to the procedure described in the preceding paper.[3]

Physical Measurements. ^{1}H NMR spectra at 500.4 MHz, ^{11}B NMR spectra at 160.5 MHz, ^{13}C NMR at 125.8 MHz, and ^{31}P NMR spectra at 202.6 MHz were obtained on a Bruker AMXII-500 spectrometer. ^{1}H NMR spectra at 200.1 MHz and ^{11}B NMR spectra at 64.2 MHz were recorded on a Bruker AC-200 spectrometer. Both spectrometers were equipped with appropriate decoupling accessories. All ^{11}B chemical shifts are referenced to external BF$_3$·O(C$_2$H$_5$)$_2$ (0.0 ppm) with a negative sign indicating an upfield shift. All ^{1}H and ^{13}C chemical shifts were measured relative to internal residual protons or carbons in the lock solvent and are referenced to Me$_4$Si (0.00 ppm). All ^{31}P chemical shifts are referenced to external 85% H$_3$PO$_4$ (0.0 ppm) with a negative sign indicating an upfield shift. Measurement of the effective magnetic moment for the paramagnetic complex **6** was accomplished with the Evan's Method[5] using a 2-mm coaxial insert. High-resolution mass spectra (HRMS) were recorded on a Micromass Autospec spectrometer. Infrared spectra were recorded on a Perkin-Elmer 1430 spectrophotometer. FT and diffuse-reflectance (DRIFT) infrared spectra were obtained on a Perkin-Elmer System 2000 FTIR spectrophotometer. Elemental analyses were performed at the University of Pennsylvania microanalysis facility. Melting points were obtained on a standard melting point apparatus and are uncorrected.

Synthesis of *exo*-6-[Mn(CO)$_5$]-*endo*-6-(C$_6$H$_5$)-*arachno*-6,7-PCB$_8$H$_{11}$ (2). To a 100-mL, two-neck, round-bottom flask equipped with a vacuum adapter, magnetic stirbar, and septum was added via syringe 6.0 mL (1.0 mmol) of a 0.17 M THF solution of *exo*-6-(C$_6$H$_5$)-*arachno*-6,7-PCB$_8$H$_{12}$ (**1a**). The flask was cooled to 0 °C and then 0.03 g (1.3 mmol) of NaH was added through one neck of the flask. After H_2 evolution ceased and ^{11}B NMR analysis of the reaction mixture indicated complete formation of 6-(C$_6$H$_5$)-*arachno*-6,7-PCB$_8$H$_{11}^-$ (**1a**$^-$), the flask was taken into the glovebag and the solution filtered to remove excess NaH. After reattaching the flask to the Schlenk line, a solution of 0.27 g (1.0 mmol) of Mn(CO)$_5$Br dissolved in 5 mL of THF was added dropwise via syringe to the solution maintained at 0 °C. After stirring for 12 h, the cloudy, yellow solution was filtered in the glovebag and the volatiles then removed from the filtrate under reduced pressure. The yellow/brown solid was dissolved in a minimum of a 1:1 CH_2Cl_2:hexanes mixture and chromatographed on a silica gel column using the same solvent mixture as eluent. Combination and concentration of appropriate fractions resulted in the isolation of *exo*-6-[Mn(CO)$_5$]-*endo*-6-(C$_6$H$_5$)-*arachno*-6,7-PCB$_8$H$_{11}$ (**2**). For **2**: R_f = 0.38; yellow solid; 0.12 g (0.29 mmol, 29%); mp 155.0−156.0 °C (dec); anal. calcd for C$_{12}$H$_{16}$B$_8$O$_5$PMn: C, 34.93; H, 3.91; found: C, 34.71; H, 3.78; ^{11}B-{^{1}H} NMR (160.5 MHz, CD_2Cl_2, ppm) 3.9 (1B), −6.3 (1B), −7.3 (1B), −13.1 (1B), −18.1 (2B), −36.2 (1B), −41.5 (1B); IR (DRIFT, KBr, cm^{-1}) 2568 (m), 2127 (w), 2051 (vs), 1966 (m), 1549 (w), 1435 (w), 1260 (w).

Similar reactions performed at −20 °C indicated the initial formation of a product which, upon warming to room temperature, rearranged to **2**. The ^{11}B{^{1}H} NMR chemical shifts for this initial compound were (64.2 MHz; THF, ppm) 5.9 (1B), −7.2 (1B), −11.0 (1B), −20.2 (2B), −27.3 (1B), −39.5 (1B), −40.7 (1B).

Synthesis of *endo*-6-[(η^5-C$_5$H$_5$)Fe(CO)$_2$]-*exo*-6-(C$_6$H$_5$)-*arachno*-6,7-PCB$_8$H$_{11}$ (3) and 1-(η^5-C$_5$H$_5$)-2-(C$_6$H$_5$)-*closo*-1,2,3-FePCB$_8$H$_9$ (4a). To a 100-mL, two-neck, round-bottom flask equipped with a vacuum adapter, magnetic stirbar, and septum was added via syringe 5.0 mL (1.0 mmol) of a 0.20 M THF solution of **1a**. The flask was cooled to 0 °C and then 0.03 g (1.3 mmol) of NaH was added through one neck of the flask. After H_2 evolution ceased and ^{11}B NMR analysis of the reaction mixture indicated complete formation of **1a**$^-$, the solution was filtered in the glovebag to remove excess NaH. The flask containing the filtrate was then reattached to the Schlenk line, and after cooling the solution to 0 °C, a sample of 0.31 g (1.0 mmol) of (η^5-C$_5$H$_5$)Fe(CO)$_2$I dissolved in 5 mL of THF was added to the solution dropwise via syringe turning the solution a dark yellow/brown color. After stirring for 12 h, the solution was filtered in the glovebag and the volatiles

(4) Shriver, D. F.; Drezdzon, M. A. *Manipulation of Air-Sensitive Compounds*, 2nd ed.; Wiley: New York, 1986.
(5) Evans, D. F. *J. Chem. Soc.* **1959**, 2003−2005. (b) Carlin, R. L. *J. Chem. Educ.* **1966**, *43*, 521−525. (c) Sur, S. K. *J. Magn. Reson.* **1989**, *82*, 169−173.

then removed from the filtrate under reduced pressure. The oily solid was dissolved in a minimum of a 1:1 CH_2Cl_2:hexanes mixture and chromatographed on a silica gel column using the same solvent mixture as eluant. Combination and concentration of appropriate fractions resulted in the isolation of two products, *endo*-6-[(η^5-C_5H_5)Fe$(CO)_2$]-*exo*-6-(C_6H_5)-*arachno*-6,7-PCB_8H_{11} (**3**) and 1-(η^5-C_5H_5)-2-(C_6H_5)-*closo*-1,2,3-$FePCB_8H_9$ (**4a**). For **3**: R_f = 0.31; orange solid; 0.23 g (0.58 mmol, 58%); mp 193.0−194.0 °C (dec); anal. calcd for $C_{14}H_{21}B_8O_2PFe$: C, 42.61; H, 5.36; found: C, 42.25; H, 5.28; HRMS (CI-) (*m*/*e*) calcd for (M-CO) $^{12}C_{13}{}^1H_{21}{}^{11}B_8{}^{18}O_1{}^{31}P_1{}^{57}Fe_1$ 368.1424, found 368.1448; ^{11}B NMR (160.5 MHz, CD_2Cl_2, ppm) 5.4 (d, 1B, J_{BH} 175), −7.1 (d, 1B, J_{BH} 155), −9.3 (d, 1B, J_{BH} 138), −17.6 (d, 1B, J_{BH} 149), −19.5 (d, 1B, J_{BH} 138), −23.1 (d, 1B, J_{BH} 146), −37.0 (d, 1B, J_{BH} 130, J_{BP} 39), −41.1 (d, 1B, J_{BH} 146); ^{1}H{^{11}B} NMR (500.4 MHz, CD_2Cl_2, ppm) 7.41−7.36 (m, C_6H_5), 4.94 (s, η^5-C_5H_5), 2.81 (s, BH), 2.63 (s, BH), 2.51 (s, BH), 2.04 (s, BH), 1.90 (s, BH), 1.85 (s, BH), 1.21 (s, CH), 0.91 (s, BH), 0.28 (s, BH), −3.24 (s, BHB), −4.44 (s, BHB); ^{31}P NMR (202.6 MHz, CD_2Cl_2, ppm) −35.3 (s, P6); IR (DRIFT, KBr, cm^{-1}) 3104 (s), 3020 (w), 2963 (w), 2567 (vs), 2030 (vs), 1987 (vs), 1821 (w), 1584 (w), 1571 (w), 1476 (m), 1434 (s), 1418 (m), 1358 (w), 1325 (w), 1262 (w), 1183 (w), 1141 (w), 1093 (m), 1071 (m), 1017 (m), 979 (w), 939 (w), 856 (s), 836 (m), 812 (m), 768 (m), 742 (m), 699 (s), 672 (m). For **4a**: R_f = 0.45; green solid; 0.007 g (0.021 mmol, 2.1%); mp 224.0−225.0 °C.; anal. calcd for $C_{12}H_{19}B_8PFe$: C, 42.82; H, 5.69; found: C, 42.70; H, 5.53; HRMS (CI-) (*m*/*e*) calcd for $^{12}C_{12}{}^1H_{19}{}^{11}B_8{}^{31}P_1{}^{57}Fe_1$ 338.1318, found 338.1321; ^{11}B NMR (160.5 MHz, CD_2Cl_2, ppm) 4.2 (d, 1B, J_{BH} 158), −0.8 (d, 1B, J_{BH} 151), −18.6 (d, 2B, J_{BH} 143), −24.5 (d, 2B, J_{BH} 184), −25.7 (d, 2B, J_{BH} 157); ^{1}H{^{11}B} NMR (500.4 MHz, CD_2Cl_2, ppm) 8.45−7.75 (m, C_6H_5), 4.77 (s, η^5-C_5H_5), 3.26 (s, BH), 2.87 (s, BH), 1.52 (s, CH), 1.41 (s, 2BH), 0.84 (s, 2BH), 0.41 (s, BH), 0.37 (s, BH); ^{31}P NMR (202.6 MHz, CD_2Cl_2, ppm) −11.3 (s, P2); IR (KBr, cm^{-1}) 3105 (m), 2537 (vs), 2509 (vs), 1480 (m), 1439 (m), 1423 (w), 1413 (m), 1333 (w), 1107 (s), 1060 (m), 1012 (w), 999 (w), 978 (w), 912 (w), 886 (w), 841 (m), 830 (w), 739 (s), 687 (s).

Photolytic Isomerization of 3 to *endo*-6-(C_6H_5)-*exo*-6-[(η^5-C_5H_5)Fe$(CO)_2$]-*arachno*-6,7-PCB_8H_{11} (5). To a quartz, 100-mL, two-neck, round-bottom flask under N_2 flow was added 0.20 g (0.5 mmol) of **3**. Acetonitrile (4 mL) was added to the flask via syringe and the flask cooled in a stream of air. The reaction solution was irradiated for a period of 3 h with a 275 W ultraviolet sunlamp which resulted in the solution slowly changing from a bright orange to a deep burgundy. The solution was taken into the glovebag and filtered, then concentrated under reduced pressure to yield *endo*-6-(C_6H_5)-*exo*-6-[(η^5-C_5H_5)Fe$(CO)_2$]-*arachno*-6,7-PCB_8H_{11} (**5**). For **5**: dark red solid; 0.15 g (0.38 mmol, 76%); anal. calcd for $C_{14}H_{21}B_8O_2PFe$: C, 42.61; H, 5.36; found: C, 42.97; H, 5.83; LRMS (CI-) (*m*/*e*) calcd for (M-CO) $^{12}C_{13}{}^1H_{21}{}^{11}B_8{}^{18}O_1{}^{31}P_1{}^{57}Fe_1$ 368; found 368; ^{11}B NMR (64.2 MHz, CH_3CN, ppm) 6.2 (d, 1B, J_{BH} 141), −5.8 (2B),[6] −13.9 (d, 1B, J_{BH} 147), −19.7 (d, 2B, J_{BH} 127), −36.3 (1B),[6] −40.5 (d, 1B, J_{BH} 139); IR (DRIFT, KBr, cm^{-1}) 2940 (m), 2910 (m), 2860 (w), 2540 (m), 1977 (s), 1410 (w), 1260 (s), 1200 (w), 1014 (s).

Synthesis of 1-(η^5-C_5H_5)-2-CH_3-*closo*-1,2,3-$FePCB_8H_9$ (4b) and 1-CH_3-2,3-(η^5-C_5H_5)$_2$-2,3,1,7-$Fe_2PCB_8H_9$ (6). In a 100-mL, round-bottom flask, 0.31 g (2.0 mmol) of *exo*-6-CH_3-*arachno*-6,7-PCB_8H_{12} (**1b**) was dissolved in 30 mL of THF under a N_2 atmosphere. To this stirred solution was added 0.048 g (2.0 mmol) of NaH. After gas evolution ceased, the solution was filtered and 0.25 g (2.0 mmol) of $FeCl_2$ and 1 mL of a 2.0 M $Na^+C_5H_5^-$/THF solution were added to the solution. After 1 h, the solution was filtered through a 1-in. plug of silica gel using CH_2Cl_2 until the eluent was colorless. The resulting solution was then evaporated to dryness. The remaining dark solid was further separated using preparative thin-layer chromatography with a 3:7 CH_2Cl_2:hexanes mixture to give two ferraphosphacarbaborane products. For **4b**: 1-(η^5-C_5H_5)-2-CH_3-*closo*-1,2,3-$FePCB_8H_9$; 0.36 g (1.32 mmol, 65.0%); blue solid; R_f = 0.55; mp 215−216 °C; anal. calcd for $C_7H_{17}B_8PFe$: C, 30.63; H, 6.24; found: C, 30.47; H, 6.09; HRMS calcd for $^{12}C_7{}^1H_{17}{}^{11}B_8{}^{31}P^{57}Fe$ (P, CI-) *m*/*e* 276.1162. found: *m*/*e* 276.1112; ^{11}B NMR (160.5 MHz, C_6D_6, ppm) 4.7 (d, 1B, J_{BH} 148), −1.9 (d, 1B, J_{BH} 150), −18.1 (d, 2B, J_{BH} 160), −22.4 (d, 2B, J_{BH} 168), −24.7 (d, 2B, J_{BH} 160); ^{1}H{^{11}B} NMR (500.4 MHz, C_6D_6, ppm) 4.32 (s, η^5-C_5H_5), 1.2 (CH_3); IR (KBr, cm^{-1}: 3215 (s), 3050 (m), 2560 (s), 1450 (s), 1255 (m), 1235 (s), 1190 (m), 1175 (w), 1070 (w), 1020 (m), 930 (m), 900 (w), 850 (w), 830 (w). For **6**: 1-CH_3-2,3-(η^5-C_5H_5)$_2$-2,3,1,7-$Fe_2PCB_8H_9$; 0.170 g (0.43 mmol, 21.6%); green solid; R_f = 0.48, mp 249−251 °C; anal. calcd for $C_{12}H_{22}B_8PFe_2$: C, 38.27; H, 6.59; Found, C, 38.09; H, 6.45; HRMS calcd for $^{12}C_{12}{}^1H_{22}{}^{11}B_8{}^{31}P^{57}Fe_2$ (P, CI-) *m*/*e* 397.0902; found: *m*/*e* 397.0927; IR (KBr, cm^{-1}) 3210 (s), 3040 (m), 2560 (s), 1450 (s), 1435 (m), 1420 (w), 1255 (s), 1195 (m), 1175 (w), 1110 (m), 990 (w), 930 (m), 880 (w), 800 (w).

Synthesis of *endo*-6-[*cis*-(Ph_3P)$_2$PtCl]-*exo*-6-(C_6H_5)-*arachno*-6,7-PCB_8H_{11} (7) and 7-(C_6H_5)-11-(Ph_3P)$_2$-*nido*-11,7,8-$PtPCB_8H_{10}$ (8). To a 100-mL, two-neck, round-bottom flask equipped with a vacuum adapter, magnetic stirbar, and septum was added via syringe 4.8 mL (1.0 mmol) of a 0.21 M THF solution of **1a**. The flask was cooled to 0 °C and then 0.03 g (1.3 mmol) of NaH was added through one neck of the flask. After H_2 evolution ceased and ^{11}B NMR analysis of the reaction mixture indicated complete formation of **1a**$^-$, the flask was taken into the glovebag and the solution filtered to remove excess NaH. After reattaching the flask to the Schlenk line, 0.79 g (1.0 mmol) of *cis*-(Ph_3P)$_2PtCl_2$ slurried in 10 mL of THF was added dropwise via syringe to the solution maintained at 0 °C. After 1 h, a solution of 0.21 g (1.0 mmol) of Proton Sponge in 4 mL of THF was added dropwise via syringe. After stirring for 12 h, the cloudy, orange solution was filtered in the glovebag and the volatiles then evaporated from the filtrate under reduced pressure. The remaining orange solid was next dissolved in a minimum of a toluene and chromatographed on a silica gel column using toluene as eluant. Combination and concentration of appropriate fractions resulted in the isolation of the two products, *endo*-6-[*cis*-(Ph_3P)$_2$PtCl]-*exo*-6-(C_6H_5)-*arachno*-6,7-PCB_8H_{11} (**7**) and 7-(C_6H_5)-11-(Ph_3P)$_2$-*nido*-11,7,8-$PtPCB_8H_{10}$ (**8**). For **7**: R_f = 0.21; orange solid; 0.12 g (0.12 mmol, 12%); mp 182−183 °C; anal. calcd for $C_{43}H_{46}B_8P_3ClPt$: C, 53.09; H, 4.77; found: C, 52.50; H, 4.67; ^{11}B{^{1}H} (64.2 MHz, CD_2Cl_2, ppm) 3.3 (1B), −2.8 (1B), −5.2 (1B), −7.9 (1B), −14.5 (1B), −20.7 (1B), −39.7 (2B); ^{1}H (200.1 MHz, CD_2Cl_2, ppm) 8.10−7.16 (m, Ph), 1.72 (s, CH), −1.1 (s, BHB), −3.5 (s, BHB); IR (DRIFT, KBr, cm^{-1}) 3053 (s), 3005 (w), 2553 (vs), 2527 (vs), 2261 (w), 1966 (w), 1900 (w), 1814 (w), 1587 (w), 1574 (w), 1480 (vs), 1435 (vs), 1377 (w), 1313 (w), 1284 (w), 1189 (m), 1160 (w), 1093 (s), 1069 (w), 999 (w), 971 (w), 943 (w), 834 (w), 810 (w), 745 (s), 700 (s). For **8**: R_f = 0.48; orange solid; 0.14 g (0.14 mmol, 14%); mp 211.0−212.0 °C; anal. calcd for $C_{43}H_{45}B_8P_3Pt$: C, 55.16; H, 4.84; found: C, 55.10; H, 4.92; ^{11}B{^{1}H} (64.2 MHz, CD_2Cl_2, ppm) 9.1 (1B), 4.0 (1B), −13.1 (1B), −18.4 (2B), −21.2 (1B), −30.0 (1B), −38.2 (1B, J_{BP} 54); ^{1}H (200.1 MHz, CD_2Cl_2, ppm) 7.56−7.03 (m, Ph), 2.92 (s, CH); IR (DRIFT, KBr, cm^{-1}) 3075 (s), 3054 (s), 3034 (s), 3005 (w), 2576 (vs), 2531 (vs), 1955 (m), 1898 (m), 1818 (m), 1660 (w), 1586 (m), 1572 (m), 1478 (vs), 1434 (vs), 1306 (m), 1184 (m), 1160 (m), 1093 (s), 1014 (m), 999 (m), 913 (w), 877 (w), 808 (w), 776 (w), 742 (s).

Crystallographic Data for 2, 3, 4a, 4b, 6, 7, and 8. Crystals of **2** (Upenn #3144) were grown by slow evaporation of a CH_2Cl_2/hexanes solution at −25 °C in the glovebox. Crystals of **3** (Upenn #3142), **7** (Upenn #3155), and **8** (Upenn #3153) were grown by slow evaporation of CH_2Cl_2/hexanes solutions in the refrigerator. Crystals of **4a** (Upenn #3067), **4b** (Upenn #3066), and **6** (Upenn #3082) were grown by slow evaporation of CH_2Cl_2/hexanes solutions at room temperature.

Collection and Reduction of the Data. X-ray intensity data were collected on a Rigaku R-AXIS IIc area detector employing graphite-monochromated Mo−K_α radiation (λ = 0.71069 Å) at temperatures of 296 K for **2**, 200 K for **3**, 295 K for **4a**, **4b**, and **6**, and 210 K for **7** and

(6) The coupling constant could not be accurately measured.

Table 1. Crystallographic Data Collection and Structure Refinement Information

	2	**3**	**4a**	**4b**	**6**	**7**	**8**
formula	$C_{12}B_8H_{16}MnPO_5$	$FeC_{14}B_8H_{21}PO_2$	$FeC_{12}PB_8H_{19}$	$FeC_7H_{17}PB_8$	$Fe_2C_{12}B_8H_{22}P$	$Pt_2C_{91}B_{16}H_{102}P_6Cl_{12}$	$PtC_{43}B_8H_{45}P_3$
formula weight	412.64	394.61	336.57	274.51	395.45	2370.09	936.27
crystal class	monoclinic	orthorhombic	triclinic	monoclinic	monoclinic	monoclinic	triclinic
space group	$P2_1/c$ (No. 14)	$P2_12_12_1$ (No. 19)	$P\bar{1}$ (No. 2)	$C2/c$ (No. 15)	$P2_1/n$ (No. 14)	$P2_1/n$ (No. 14)	$P\bar{1}$ (No. 2)
Z	4	4	2	8	4	2	2
cell constants							
a (Å)	10.13070(10)	11.8876(3)	7.8825(3)	26.0242(6)	9.2231(2)	12.4084(1)	11.9097(2)
b (Å)	14.8154(4)	17.2869(4)	16.0671(6)	8.1266(1)	13.4955(3)	18.0854(2)	17.2245(4)
c (Å)	13.2955(3)	9.3156(3)	6.9036(2)	14.3484(2)	13.9081(3)	22.7549(3)	10.7383(3)
α (deg)			96.392(3)				99.385(1)
β (deg)	101.577(2)		106.633(2)	120.364(1)	96.117(1)	97.6160(7)	107.444(2)
γ (deg)			78.401(2)				88.530(2)
V (Å^3)	1954.93(7)	1914.35(9)	819.29(5)	2618.29(8)	1721.29(7)	5061.4(1)	2072.77(8)
μ (cm^{-1})	7.76	8.76	10.02	12.36	17.65	32.17	35.32
min and max trans				0.619, 1.010	0.733, 1.001		
crystal size, mm	0.45 × 0.20 × 0.05	0.45 × 0.12 × 0.08	0.70 × 0.30 × 0.05	0.40 × 0.08 × 0.03	0.25 × 0.18 × 0.05	0.32 × 0.26 × 0.26	0.36 × 0.30 × 0.22
D_{calc} (g/cm^3)	1.402	1.369	1.364	1.393	1.526	1.555	1.500
F(000)	832	808	344	1120	804	2356	932
radiation	Mo Kα (λ = 0.71069 Å)	Mo Kα (λ = 0.71069 Å)	Mo Kα (λ = 0.71069 Å)	Mo Kα (λ = 0.71069 Å)	Mo Kα (λ = 0.71069 Å)	Mo Kα (λ = 0.71069 Å)	Mo Kα (λ = 0.71069 Å)
2θ range (deg)	5.38−50.7	5.56−50.7	5.18−49.9	3.62−49.86	5.38−49.62	5.1−54.96	5.02−54.96
hkl collected	$-11 \le h \le 11$, $-17 \le k \le 17$, $-15 \le l \le 16$	$-14 \le h \le 14$, $-20 \le k \le 20$, $-10 \le l \le 11$	$-9 \le h \le 9$, $-19 \le k \le 19$, $-8 \le l \le 8$	$-30 \le h \le 30$, $-9 \le k \le 8$, $-17 \le l \le 17$	$-10 \le h \le 9$, $-15 \le k \le 15$, $-16 \le l \le 16$	$-15 \le h \le 16$, $-23 \le k \le 22$, $-29 \le l \le 29$	$-15 \le h \le 14$, $-22 \le k \le 22$, $-13 \le l \le 13$
no. reflns measd	12515	12147	6868	9841	8866	51924	34306
no. unique reflns	3425 (R_{int} = 0.0383)	3478 (R_{int} = 0.0458)	2654 (R_{int} = 0.0328)	2279 (R_{int} = 0.0471)	2794 (R_{int} = 0.0395)	11434 (R_{int} = 0.0424)	9416 (R_{int} = 0.0408)
no. obsd reflns	3053 ($F > 4\sigma$)	3306 ($F > 4\sigma$)	2467 ($F > 4\sigma$)	2084 ($F > 4.0\sigma$)	2527 ($F > 4\sigma$)	10550 ($F > 4\sigma$)	9055 ($F > 4\sigma$)
no. reflns used in refinement	3425	3478	2654	2279	2794	11434	9416
no. parameters	288	280	235	190	256	549	537
R indices ($F > 4\sigma$)[a]	$R_1 = 0.0476$ w$R_2 = 0.0910$	$R_1 = 0.0323$ w$R_2 = 0.0647$	$R_1 = 0.0398$ w$R_2 = 0.1046$	$R_1 = 0.0495$ w$R_2 = 0.0834$	$R_1 = 0.0399$ w$R_2 = 0.0805$	$R_1 = 0.0480$ w$R_2 = 0.1228$	$R_1 = 0.0370$ w$R_2 = 0.0911$
R indices (all data)	$R_1 = 0.0568$ w$R_2 = 0.0948$	$R_1 = 0.0360$ w$R_2 = 0.0666$	$R_1 = 0.0435$ w$R_2 = 0.1074$	$R_2 = 0.0566$ w$R_2 = 0.0859$	$R_2 = 0.0474$ w$R_2 = 0.0844$	$R_1 = 0.0528$ w$R_2 = 0.1275$	$R_1 = 0.0399$ w$R_2 = 0.0938$
GOF	1.171	1.141	1.067	1.170	1.118	1.088	1.057
final difference peaks, e/Å^3	+0.187, −0.251	+0.275, −0.318	+0.52, −0.33	+0.24, −0.29	+0.25, −0.27	+1.087, −2.265	+1.358, −1.089

[a] $R_1 = \sum||F_o| - |F_c||/\sum|F_o|$; w$R_2 = \{\sum w(F_o^2 - F_c^2)^2/\sum w(F_o^2)^2\}^{1/2}$.

8. Indexing was performed from a series of 1° oscillation images. Depending upon the specific compound, a hemisphere of data was collected using 5°, 6°, or 8° oscillation angles with exposures of 120−250 s per frame and a crystal-to-detector distance of 82 mm. Oscillation images were processed using bioteX,[7] producing a listing of unaveraged F^2 and $\sigma(F^2)$ values which were then passed to the teXsan[8] program package for further processing and structure solution on a Silicon Graphics Indigo R4000 computer. The intensity data for **2**, **3**, **4a**, **4b**, and **6** were corrected for Lorentz and polarization effects but not for absorption. The intensity data for **7** and **8** were corrected for Lorentz and polarization effects and for absorption using REQAB[9] (minimum and maximum transmission for **7**: 0.619 and 1.010; for **8**: 0.733 and 1.010).

Solution and Refinement of the Structures. The structures were solved by direct methods (SIR92[10]). The structure of **7** includes 2.5 molecules of dichloromethane solvent per asymmetric unit (one molecule lies on a center of symmetry). The data were corrected for disordered solvent using SQUEEZE.[11] Refinement for all compounds was by full-matrix least squares based on F^2 using SHELXL-93.[12] All reflections were used during refinement (F^2's that were experimentally negative were replaced by $F^2 = 0$). The weighting scheme used was $w = 1/[\sigma^2(F_o^2) + aP^2 + bP]$ where $P = (F^2_o + 2F^2_c)/3$. For **3** and **8**, non-hydrogen atoms were refined anisotropically, cage hydrogen atoms were refined isotropically, and all other hydrogen atoms were refined using a "riding" model. For **2**, **4a**, **4b**, **6**, and **7**, non-hydrogen atoms were refined anisotropically, cage hydrogen atoms were refined isotropically, and all other hydrogen atoms were included as constant contributions to the structure factors and were not refined. Crystal and refinement data are given in Table 1. Selected intramolecular bond distances and angles are given in the figure captions.

(7) *bioteX*: A suite of Programs for the Collection, Reduction, and Interpretation of Imaging Plate Data, Molecular Structure Corporation, 1995.
(8) *teXsan*: Crystal Structure Analysis Package, Molecular Structure Corporation, 1985 & 1992.
(9) *REQAB4*: Jacobsen, R. A. Private Communication, 1994.
(10) *SIR92*: Altomare, A.; Burla, M. C.; Camalli, M.; Cascarano, M.; Giacovazzo, C.; Guagliardi, A.; Polidoro, G. *J. Appl. Cryst.* **1994**, *27*, 435.
(11) *SQUEEZE*: Sluis, P. v. d.; Spek, A. L. *Acta Cryst.* **1990**, *A46*, 194.
(12) Sheldrick, G. M. *SHELXL-93*: *Program for the Refinement of Crystal Structures*; University of Göttingen: Göttingen, Germany, 1993.

Results and Discussion

The compositions of all compounds were established by exact mass determinations or elemental analyses and the structures of complexes **2**, **3**, **4a**, **4b**, **6**, **7,** and **8** were crystallographically confirmed.

Reaction of 6-(C_6H_5)-*arachno*-6,7-$PCB_8H_{11}^-$ (**1a**$^-$) with $Mn(CO)_5Br$ (eq 1) resulted in the formation of a single product **2** containing a coordinated $Mn(CO)_5$ fragment.

$$\underset{\mathbf{1a}^-}{Na^+[6\text{-}(C_6H_5)\text{-}arachno\text{-}6,7\text{-}PCB_8H_{11}{}^-]} + Mn(CO)_5Br \rightarrow \underset{\mathbf{2}}{exo\text{-}6\text{-}[Mn(CO)_5]\text{-}endo\text{-}6\text{-}(C_6H_5)\text{-}arachno\text{-}6,7\text{-}PCB_8H_{11}} + NaBr \quad (1)$$

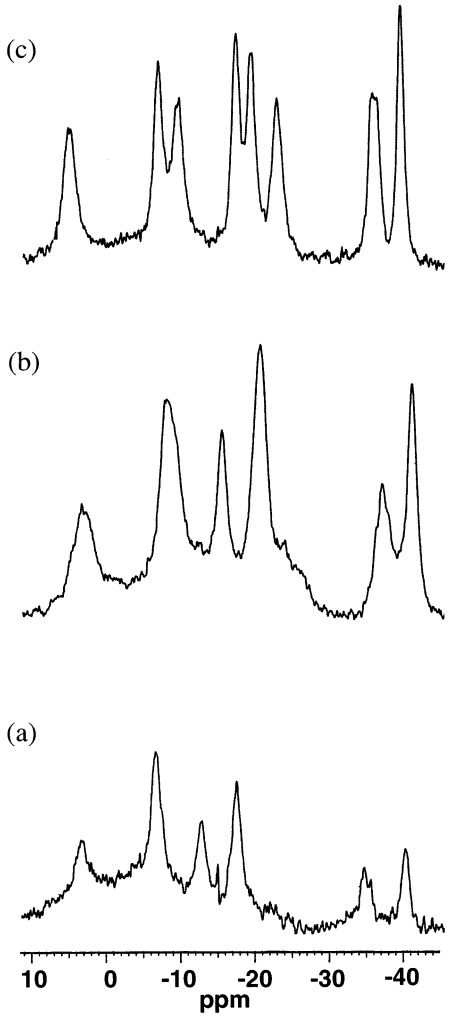

Figure 3. Comparison of 64.2 MHz $^{11}B\{^1H\}$ NMR spectra for (a) *exo*-6-[$Mn(CO)_5$]-*endo*-6-(C_6H_5)-*arachno*-6,7-PCB_8H_{11} (**2**), (b) *exo*-6-[(η^5-C_5H_5)$Fe(CO)_2$]-*endo*-6-(C_6H_5)-*arachno*-6,7-PCB_8H_{11} (**5**), and (c) *endo*-6-[(η^5-C_5H_5)$Fe(CO)_2$]-*exo*-6-(C_6H_5)-*arachno*-6,7-PCB_8H_{11} (**3**).

Reaction of **1a**$^-$ with (η^5-C_5H_5)$Fe(CO)_2I$ (eq 2) yielded two products, **3** and **4a**, one having a coordinated (η^5-C_5H_5)$Fe(CO)_2$ fragment, with the other containing only a (η^5-C_5H_5)Fe unit.

$$2\ Na^+[6\text{-}(C_6H_5)\text{-}arachno\text{-}6,7\text{-}PCB_8H_{11}^-] + 2\ (\eta^5\text{-}C_5H_5)Fe(CO)_2I \rightarrow$$
$$\mathbf{1a}^-$$
$$2\text{-}x\ endo\text{-}6\text{-}[(\eta^5\text{-}C_5H_5)Fe(CO)_2]\text{-}exo\text{-}6\text{-}(C_6H_5)\text{-}arachno\text{-}6,7\text{-}PCB_8H_{11} +$$
$$\mathbf{3}$$
$$x\ 1\text{-}(\eta^5\text{-}C_5H_5)\text{-}2\text{-}(C_6H_5)\text{-}closo\text{-}1,2,3\text{-}FePCB_8H_9 +$$
$$\mathbf{4a}$$
$$2x\ CO + x\ H_2 + 2\ NaI \quad (2)$$

As shown in Figure 3, the ^1H-decoupled 64.2 MHz ^{11}B NMR spectra of **2** and **3** are both indicative of C_1 symmetric structures, with that of **2** (Figure 3a) showing six peaks of relative intensities 1:2:1:2:1:1[13] and that of **3** (Figure 3c) showing eight equal-intensity resonances. The peak at −37.0 ppm in the spectrum of **3** displayed boron−phosphorus fine coupling (J_{BP} = 39 Hz) consistent with that boron being situated in a position adjacent to the cage phosphorus. As shown in Figures 4 and 5, single-crystal X-ray investigations established that, indeed, both complexes had C_1 symmetry and contained 6-(C_6H_5)-*arachno*-6,7-$PCB_8H_{11}^-$ phosphamonocarbaborane ligands bonded in η^1-fashions to the metal atoms, but, surprisingly, the compounds differ in that the $Mn(CO)_5$ unit in **2** is bonded at the *exo*-P6 position, while the (η^5-C_5H_5)$Fe(CO)_2$ group in **3** is attached at the *endo*-P6 position!

(13) As given in the Experimental Section, the 160.5 MHz 11B NMR spectrum of **2** resolves into seven peaks of relative intensities 1:1:1:1:2:1:1.

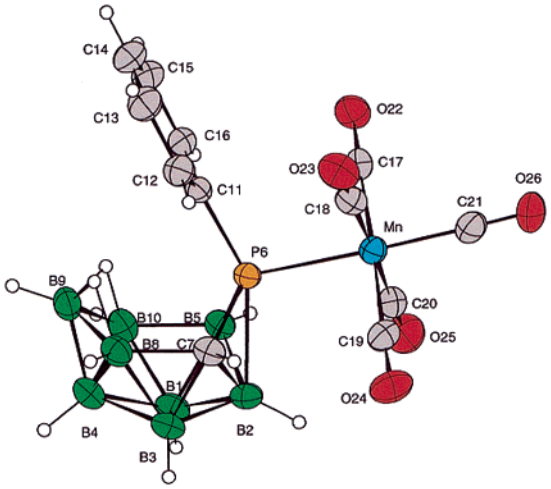

Figure 4. ORTEP representation (30% probability ellipsoids) of *exo*-6-[$Mn(CO)_5$]-*endo*-6-(C_6H_5)-*arachno*-6,7-PCB_8H_{11} (**2**). Selected bond lengths (Å) and angles (°): P6−Mn, 2.4012(9); P6−B2, 2.235(4); P6−C7, 1.838-(3); P6−B5, 1.898(4); B5−B10, 1.783(5); C7−B8, 1.701(5); B8−B9, 1.803-(6); B9−B10, 1.814(6); Mn−C21, 1.847(4); Mn−C17, 1.869(3); Mn−C18, 1.873(4); Mn−C19, 1.860(4), Mn−C20, 1.866(4); Mn−P6−B2, 102.70-(11); Mn−P6−C11, 106.64(9); Mn−P6−C7, 116.25(11); Mn−P6−B5, 116.89(12); P6−Mn−C21, 177.27(12); C11−P6−B2, 150.38(14).

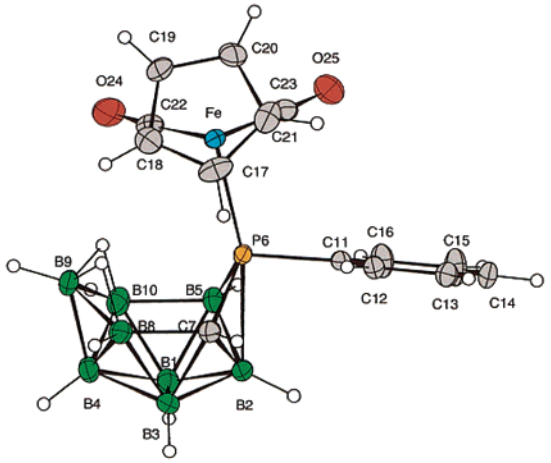

Figure 5. ORTEP representation (30% probability ellipsoids) of *endo*-6-[(η^5-C_5H_5)$Fe(CO)_2$]-*exo*-6-(C_6H_5)-*arachno*-6,7-PCB_8H_{11} (**3**). Selected bond lengths (Å) and angles (°): P6−Fe, 2.3075(8); P6−B2, 2.232(3); P6−C7, 1.846(3); P6−B5, 1.909(3); B5−B10, 1.791(5); C7−B8, 1.681(4); B8−B9, 1.816(5); B9−B10, 1.826(5); Fe−C22, 1.764(3); C22−O24, 1.145(4); Fe−C23, 1.765(3); C23−O25, 1.148(4); Fe−P6−B2, 166.64(9); Fe−P6−C11, 105.29(8); Fe−P6−C7, 121.64(10), Fe−P6−B5, 124.76(11); C11−P6−B2, 87.76(12); P6−Fe−C23, 87.83(11); P6−Fe−C22, 96.35(11); C22−Fe−C23, 92.37(14).

The bond lengths and angles in the phosphamonocarbaborane units in both **2** and **3** are quite similar and thus do not appear to be affected by either the identity or the endo or exo position of the metal fragment at the P6 site. For example, even though P6−B2 is cis to the Mn−P6 bond in **2** and trans to the Fe−P6 bond in **3**, it has experimentally identical lengths in both compounds, 2.235(4) Å in **2** and 2.232(3) Å in **3**. Likewise, the Mn−P6−C11 (106.64(9)°) and Fe−P6−C11 (105.29(8)°) bond angles are nearly identical. In **2**, the Mn atom lies in the

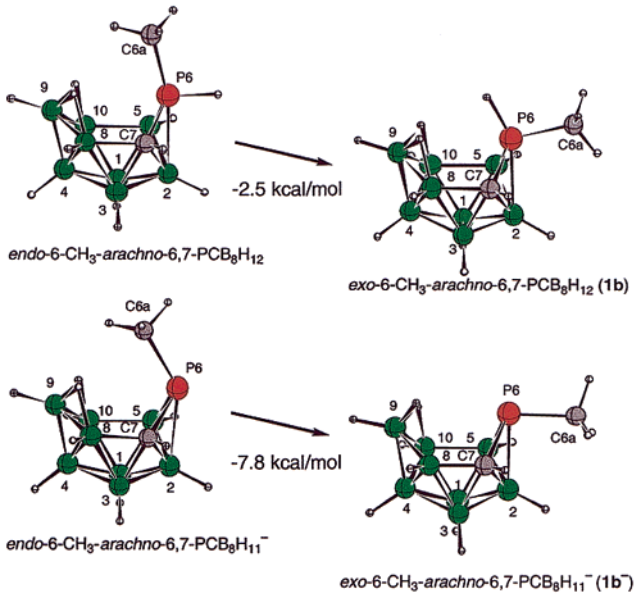

Figure 6. DFT optimized geometries and relative energies for endo and exo isomers of both **1b** and **1b**$^-$.

P6−B2−B4−B9 plane. Likewise, even though the (η^5-C_5H_5)-$Fe(CO)_2$ fragment in **3** is oriented across the P6−B2−B4−B9 plane, the Fe atom still remains in this plane. In **2**, the $Mn(CO)_5$ unit has no significant interactions with the cage, but in **3**, the C18-hydrogen and the B8,9-H bridge-hydrogen and the C22 carbonyl carbon and the B9,10-H bridge-hydrogen are separated by only 2.43(3) and 2.42(4) Å, respectively. The P6−Mn bond in **2** is trans to the C(21)≡O(26) carbonyl (P6−Mn−C21, 177.27(12)°) with the remaining carbonyls in the perpendicular plane passing through the Mn. The Mn−C21 bond is shorter, 1.847(4) Å than any of the Mn−CO lengths to the other four carbonyls (1.867(4) Å average) consistent with stronger Mn to C21 back-bonding which could result from the *trans*-phosphamonocarbaborane being a better donor than a *trans*-carbon monoxide.

When the reaction of **1a**$^-$ with $Mn(CO)_5Br$ was carried out at −20 °C, the initial formation of another compound was observed, which then cleanly converted to **2** upon warming to room temperature. The ^{11}B {^1H} NMR spectrum for this initial, unstable product (5.9, −7.2, −11.0, −20.2, −27.3, −39.5, −40.7 ppm, in 1:1:1:2:1:1:1 ratios) is, in fact, quite similar to that found for *endo*-6-[(η^5-C_5H_5)$Fe(CO)_2$]-*exo*-6-(C_6H_5)-*arachno*-6,7-PCB_8H_{11} (**3**) (Figure 3c) suggesting that at low temperatures, *endo*-6-[$Mn(CO)_5$]-*exo*-6-(C_6H_5)-*arachno*-6,7-PCB_8H_{11} is formed, but that this compound then rearranges upon warming to room temperature to afford the isolated *exo*-6-[$Mn(CO)_5$]-*endo*-6-(C_6H_5)-*arachno*-6,7-PCB_8H_{11} (**2**) isomer. This result would seem to indicate that the exo site is energetically more favorable for a metal substituent than the endo position.

The lone pair remaining at the phosphorus upon deprotonation of *exo*-6-R-*arachno*-6,7-PCB_8H_{12} (**1**) with base to form the **1**$^-$ anion could, in fact, be situated in either an endo or exo orientation. As depicted in Figure 6, density functional calculations at the B3LYP/6-311G* level of the possible endo and exo isomers of the **1b**$^-$ anion established that the isomer with the lone pair in the endo position is energetically favored by 7.8 kcal/mol, strongly supporting initial attack by electrophiles at the endo position. This conclusion is further supported by the observation reported in the preceding paper[3] that when **1a**$^-$ was reacted with O_2, S_8, BH_3·THF, or Br_2, the resulting *endo*-6-O-*exo*-6-(C_6H_5)-*arachno*-6,7-$PCB_8H_{11}^-$, *endo*-6-S-*exo*-6-(C_6H_5)-*arachno*-6,7-$PCB_8H_{11}^-$, *endo*-6-BH_3-*exo*-6-(C_6H_5)-*arachno*-6,7-$PCB_8H_{11}^-$, and *endo*-6-Br-*exo*-6-(C_6H_5)-*arachno*-6,7-PCB_8H_{11} products were substituted at the endo positions.

DFT calculations on the model compounds, *endo*-6-CH_3-*arachno*-6,7-PCB_8H_{12} and *exo*-6-CH_3-*arachno*-6,7-PCB_8H_{12} also showed (Figure 6) that for these neutral substituted compounds the exo site was favored by the methyl substituent by 2.5 kcal/mol. Naturally, because of the reduction in steric interactions, it would be expected that the exo site would be even more favored than the endo position for larger groups, such as $Mn(CO)_5$ and (η^5-C_5H_5)$Fe(CO)_2$. Therefore, while initial reactions with these metal electrophiles probably occur at the endo position, the calculations indicate that the resulting endo-substituted isomers should be unstable with respect to rearrangement to exo isomers in which these large groups can adopt a sterically less demanding environment.

The above observations and conclusions led to the prediction that *endo*-6-[(η^5-C_5H_5)$Fe(CO)_2$]-*exo*-6-(C_6H_5)-*arachno*-6,7-PCB_8H_{11} (**3**) should be unstable with respect to rearrangement to its exo-substituted isomer. While it was not possible to thermally induce this isomerization, it was found that when an acetonitrile solution of **3** was photolyzed with UV-radiation, conversion to *exo*-6-[(η^5-C_5H_5)$Fe(CO)_2$]-*endo*-6-(C_6H_5)-*arachno*-6,7-PCB_8H_{11} (**5**) (eq 3) occurred.

$$\underset{\mathbf{3}}{\textit{endo}\text{-6-}[(\eta^5\text{-}C_5H_5)Fe(CO)_2]\text{-}\textit{exo}\text{-6-}(C_6H_5)\text{-}\textit{arachno}\text{-6,7-}PCB_8H_{11}} \xrightarrow[CH_3CN]{h\nu} \underset{\mathbf{5}}{\textit{exo}\text{-6-}[(\eta^5\text{-}C_5H_5)Fe(CO)_2]\text{-}\textit{endo}\text{-6-}(C_6H_5)\text{-}\textit{arachno}\text{-6,7-}PCB_8H_{11}} \quad (3)$$

The ^1H-decoupled ^{11}B NMR spectra for compounds **2**, **3**, and **5** are compared in Figure 3, where it can be seen that, while all three spectra are generally similar, the spectra of **2** (Figure 3a) and **5** (Figure 3b) are nearly identical, strongly indicating that isomerization of the (η^5-C_5H_5)$Fe(CO)_2$ fragment to the *exo*-P6 position has occurred. For example, unlike in the spectrum of **3** (Figure 3c), both **2** and **5** exhibit a resonance near −13 ppm. Likewise, **3** contains a peak at −23.1 ppm which is not present in the spectra of either **2** or **5**.

In the η^1-complexes **2**, **3**, **5**, and **7** (vide infra), the 6-R-*arachno*-6,7-$PCB_8H_{11}^-$ is coordinated to the metals by a metal-phosphorus single bond. Thus, in these cases the phosphamonocarbaboranyl anion is functioning as a simple two-electron sigma donor and, as such, it can be considered an anionic equivalent of a phosphine. This anion could also be considered to be an analogue of Fu's diphenylphosphidoboratabenzene $(P(BC_5H_5)(C_6H_5)_2)^-$ anion, which has also been shown to form the (η^5-C_5H_5)$Fe(CO)_2$[$P(BC_5H_5)(C_6H_5)_2$] analogue of complex **3**.[14] The CO stretching frequencies in **3** (KBr, 2030 and 1987 cm^{-1}) are higher than those found for either (η^5-C_5H_5)$Fe(CO)_2$-[$P(BC_5H_5)(C_6H_5)_2$] (KBr, 2024 and 1982 cm^{-1}) or (η^5-C_5H_5)-$Fe(CO)_2(PPh_2)$ (cyclohexane, 2015, 1966 cm^{-1})[15] indicating that **1b**$^-$ is less electron donating than either the $(PPh_2(BC_5H_5))^-$ or PPh_2^- anions.

Consistent with the above differences in CO stretching frequencies, the Fe−P6 bond distance in **3** is longer (2.3075(8) Å) than the Fe−P bond in (η^5-C_5H_5)$Fe(CO)_2$[$P(BC_5H_5)(C_6H_5)_2$]

(2.276(2) Å). Likewise, the Fe−CO bond lengths in **3** are longer (1.765(3) and 1.764(3) Å) and the C≡O lengths shorter (1.145(4) and 1.148(4) Å) than those in (η^5-C_5H_5)Fe(CO)$_2$[P(BC_5H_5)(C_6H_5)$_2$] (Fe−CO, 1.741(10) and 1.743(10) Å); C≡O, 1.170(9) and 1.167(9) Å). The Fe−P6 distance in **3** is also much longer than the Fe−P distance (2.188(3) Å) observed in [3-(CO)-3-$COCH_3$-3-$P(CH_3)_3$-*closo*-3,1,2-$FeC_2B_9H_{11}$]$^-$.[16]

The other compound that was isolated from the reaction of **1a**$^-$ with (η^5-C_5H_5)Fe(CO)$_2$I (eq 3) was characterized as 1-(η^5-C_5H_5)-2-(C_6H_5)-*closo*-1,2,3-$FePCB_8H_9$ (**4a**). The methyl-substituted analogue of this compound, 1-(η^5-C_5H_5)-2-CH_3-*closo*-1,2,3-$FePCB_8H_9$ (**4b**), along with the new diiron cluster, 1-CH_3-2,3-(η^5-C_5H_5)$_2$-2,3,1,7-$Fe_2PCB_8H_9$ (**6**), was obtained by the reaction of $FeCl_2$ and $Na^+C_5H_5^-$with 6-CH_3-*arachno*-6,7-$PCB_8H_{11}^-$ (**1b**$^-$). (eq 4)

$$4\ Na^+[6\text{-}CH_3\text{-}arachno\text{-}6,7\text{-}PCB_8H_{11}^-] + 6\ Na^+C_5H_5^- + \underset{\mathbf{1b}^-}{}$$
$$5\ FeCl_2 \xrightarrow[-10\ NaCl]{-4\ H_2}$$
$$4\text{-}x\ 1\text{-}(\eta^5\text{-}C_5H_5)\text{-}2\text{-}CH_3\text{-}closo\text{-}1,2,3\text{-}FePCB_8H_9 + \underset{\mathbf{4b}}{}$$
$$x\ 1\text{-}CH_3\text{-}2,3\text{-}(\eta^5\text{-}C_5H_5)_2\text{-}2,3,1,7\text{-}Fe_2PCB_8H_9 \quad (4)$$
$$\underset{\mathbf{6}}{}$$

The ^{11}B NMR spectra of **4a** and **4b** each consist of five doublet resonances with relative intensity ratios of 1:1:2:2:2, indicating that, in contrast to the C_1 symmetry of the **1a**$^-$ and **1b**$^-$ anions, the complexes have C_S symmetry. On the basis of skeletal electron-counting rules,[17] a cluster of the formula, 1-(η^5-C_5H_5)-2-R-*closo*-1,2,3-$FePCB_8H_9$, has 24 skeletal electrons and would be expected to adopt an 11-vertex, *closo*-octadecahedral geometry similar to that which has been confirmed for the isoelectronic tricarbadecaboranyl 1-(η^5-C_5H_5)-2-R-*closo*-1,2,3,4-$FeC_3B_7H_9$ complexes.[18]

The structures of both **4a** and **4b** were crystallographically established, but since there are no significant structural differences, only the structure of **4b** is shown in Figure 7. Consistent with the skeletal electron-counting prediction, the $FePCB_8$ cluster adopts the closo-octadecahedral structure with the iron atom occupying the unique six-coordinate vertex over the puckered open face of the phosphamonocarbaboranyl ligand. Compounds **4a** and **4b** and the isoelectronic tricarbadecaboranyl complex,[18] 1-(η^5-C_5H_5)-2-R-*closo*-1,2,3,4-$FeC_3B_7H_9$, can also be considered as ferrocene analogues, in which an Fe(II) ion is sandwiched between a $C_5H_5^-$ and either the R-*nido*-$PCB_8H_9^-$ or R-*nido*-$C_3B_7H_9^-$ ligands, respectively. The *nido*-phosphamonocarbaboranyl ligand was apparently formed by a process, such as shown in path d in Figure 2, involving loss of molecular hydrogen (and as a result, two electrons) from **1b**$^-$ during the iron insertion reaction. However, the R-*nido*-$PCB_8H_9^-$ cluster framework in **4a** and **4b** does not have the C_1 symmetry indicated in Figure 2, but instead has C_S symmetry, where the carbon that was adjacent to the phosphorus in **1** has migrated away from the phosphorus to a 4-coordinate cage position adjacent to the Fe atom. Thus, complexes **4a** and **4b** are actually derivatives of the 6-CH_3-*nido*-6,9-$PCB_8H_9^-$ anion that was structurally characterized in the preceding paper.[3] The observed carbon rearrangement is consistent with the well-established preference[18,19] of carbon atoms to occupy lower coordinate vertices in carborane and metallacarborane clusters, and similar carbon migration reactions have, in fact, been previously observed in the isoelectronic 11-vertex metallatricarbadecaboranyl complexes.[20]

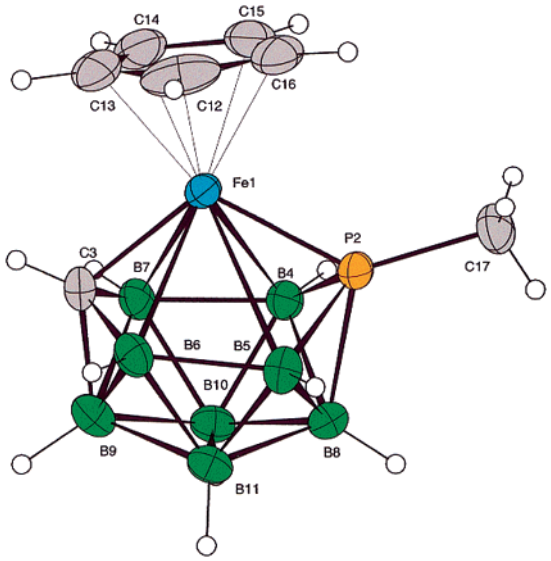

Figure 7. ORTEP representation (30% probability ellipsoids) of 1-(η^5-C_5H_5)-2-CH_3-*closo*-1,2,3-$FePCB_8H_9$ (**4b**). Selected bond lengths (Å) and angles (°): Fe−P2, 2.1342(10); Fe−C3, 1.955(4); Fe−B6, 2.373(4); Fe−B7, 2.297(4); Fe−B4, 2.391(4); Fe−B5, 2.636(5); C3−B7, 1.592(5); B7−B4, 1.832(5); B4−P2, 1.894(4); P2−B5, 1.868(5); B5−B6, 1.860(6); Fe−P2−C17, 135.93(14).

The shortest distances between the iron and the phosphamonocarbaboranyl ligand are to the carbon (C3) and phosphorus (P2) atoms that are puckered out of the six-membered face toward the iron atom. The Fe−C3 length (1.955(4) Å) in **4b** is similar to that found for the corresponding Fe−C3 length (1.947(2) Å) in the isoelectronic ferratricarbaborane complex, 1-(η^5-C_5H_5)-2-CH_3-*closo*-1,2,3,4-$FeC_3B_7H_9$.[18] Consistent with a strong bonding interaction between the iron and phosphorus, the Fe−P2 bond length (2.1342(10) Å) is significantly shorter than the Fe−P6 length in **3** (2.3075(8) Å). Longer bond lengths are found from Fe to the remaining four boron cage atoms, with the Fe−B5 length (2.636(5) Å) being significantly longer than the Fe−B5 (2.373(4) Å), Fe−B6 (2.391(4) Å), and Fe−B7 (2.297(4) Å) lengths, so that the Fe atom is distorted 0.1682(4) Å out of the P2−B8−B9−C3 plane toward the B4−B7 edge. Similar types of distortions have previously been observed in isoelectronic 11-vertex complexes.[21]

On the basis of skeletal electron-counting rules, compound **6**, 1-CH_3-2,3-(η^5-C_5H_5)2-2,3,1,7-$Fe_2PCB_8H_9$, would be a 25

(14) Hoic, D. A.; Davis, W. M.; Fu, G. C. *J. Am. Chem. Soc.* **1996**, *118*, 8176−8177.
(15) Burckett-St. Laurent, J. C. T. R.; Haines, R. J.; Nolte, C. R.; Steen, N. D. C. T. *Inorg. Chem.* **1980**, *19*, 577−587.
(16) Lee, S. S.; Knobler, C. B.; Hawthorne, M. F. *Organometallics* **1991**, *10*, 1054−1062.
(17) (a) Wade, K. *Adv. Inorg. Chem. Radiochem.* **1976**, *18*, 1−66. (b) Williams, R. E. *Adv. Inorg. Chem. Radiochem.* **1976**, *18*, 67−142. (c) Williams, R. E. *Chem. Rev.* **1992**, *92*, 117−201. (d) Williams, R. E. In *Electron Deficient Boron and Carbon Clusters*; Olah, G. A., Wade, K., Williams, R. E., Eds.; Wiley: New York, 1991.
(18) Plumb, C. A.; Carroll, P. J.; Sneddon, L. G. *Organometallics* **1992**, *11*, 1665−1671.
(19) Bausch, J. W.; Rizzo, R. C.; Sneddon, L. G.; Wille, A. E.; Williams, R. E. *Inorg. Chem.* **1996**, *35*, 131−135.
(20) Barnum, B. A.; Carroll, P. J.; Sneddon, L. G. *Inorg. Chem.* **1997**, *36*, 1327−1337.
(21) See, for example: Plumb, C. A.; Carroll, P. J.; Sneddon, L. G. *Organometallics* **1992**, *11*, 1672−1680 and references therein.

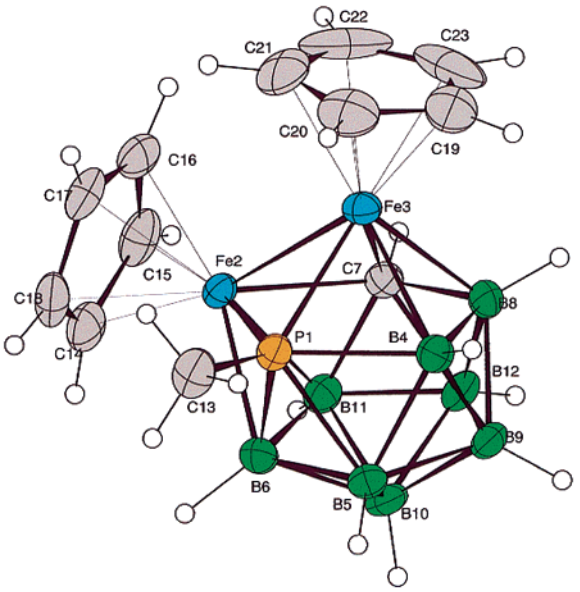

Figure 8. ORTEP representation (30% probability ellipsoids) of 1-CH_3-2,3-(η^5-C_5H_5)$_2$-2,3,1,7-$Fe_2PCB_8H_9$ (**6**). Selected bond lengths (Å): Fe2−Fe3, 2.4761(7); Fe2−P1, 2.1774(10); Fe3−P1, 2.1802(10); Fe2−C7, 2.120(4); Fe3−C7, 2.129(3); Fe2−B6, 2.158(4); Fe2−B11, 2.089(4); Fe3−B8, 2.092(4); Fe3−B4, 2.145(4); P1−B4, 2.019(4); P1−B5, 2.016(4).

skeletal-electron, 12-vertex cluster. A magnetic moment measurement using the Evan's Method for **6** was consistent with its odd electron count, indicating a single unpaired electron (μ = 1.80). Since the complex is paramagnetic, NMR spectroscopy could not be used for structural elucidation; however, the structure was crystallographically confirmed, as shown in the ORTEP drawing in Figure 8. Even though it is one electron short of the number of skeletal electrons normally needed for a closo cage geometry, **6** adopts an apparent closo icosahedral geometry with no obvious cage distortions. All of the cluster faces are triangular.

The cluster can be envisioned as formed by insertion of two (η^5-C_5H_5)Fe units into the formal R-*arachno*-$PCB_8H_9^{3-}$ fragment. Since **6** is neutral, this requires that the two iron atoms be in formal Fe^{II} and Fe^{III} oxidation states. However, the structural determination shows no apparent differences in the bonding configuration of the two iron atoms, suggesting that they have averaged oxidation states. For example, both Fe atoms exhibit similar Fe to C_5H_5-ring centroid distances (1.7277(4) and 1.7266(4) Å). Likewise, both Fe atoms are in identical five-coordinate cluster sites and exhibit similar bond distances to their neighboring cluster atoms. The Fe−Fe bond length (2.4761(7) Å) in **6** is shorter than those found in either of the diferradicarbaborane complexes, 1,6-[(η^5-C_5H_5)Fe]2-2,3-$C_2B_6H_8$ (2.571(1) Å, Fe^{III}−Fe^{III})[22] or $(CO)_4Fe_2^{I}(1,2\text{-}C_2B_9H_{11})_2^{2-}$ (2.591(5) Å, Fe^{I}−Fe^{I}),[23] but longer than the Fe−Fe distance (2.414(4) Å) observed in the mixed-spin Fe^{II}−Fe^{II} bond in the "wedged" metallacarborane, [2,3-$(CH_3)_2C_2B_4H_4]_2Fe_2^{II}(OCH_3)_2$-$C_2H_4$.[24]

As in **4a** and **4b**, the carbon and phosphorus atoms in **6** have separated from their adjacent positions in the starting $\mathbf{1b}^-$ anion to generate a C_S symmetric structure in which these atoms bridge

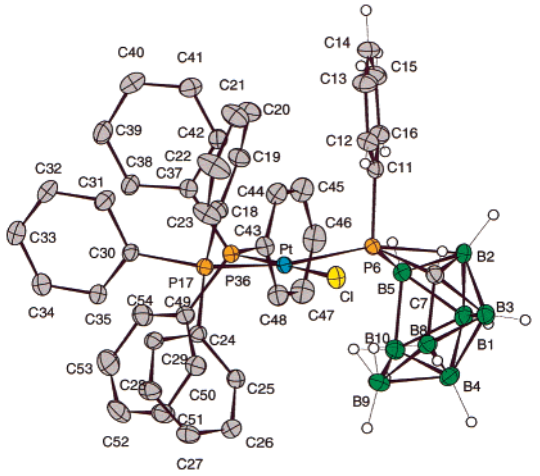

Figure 9. ORTEP representation (30% probability ellipsoids) of *endo*-6-[*cis*-$(Ph_3P)_2PtCl$]-*exo*-6-(C_6H_5)-*arachno*-6,7-PCB_8H_{11} (**7**). Selected bond lengths (Å) and angles (°): P6−Pt, 2.3636(12); P6−B2, 2.233(5); P6−C7, 1.843(5); P6−B5, 1.918(6); B5−B10, 1.823(8); C7−B8, 1.660(8); B8−B9, 1.811(9); B9−B10, 1.822(9); Pt−P36, 2.2516(12); Pt−P17, 2.3782(12); Pt−Cl, 2.3601(12); Pt−P6−B2, 161.7(2); Pt−P6−C11, 100.4(2); Pt−P6−C7, 114.1(2); Pt−P6−B5, 131.2(2); C11−P6−B2, 93.4(2); P6−Pt−P36, 94.61(4); P36−Pt−P17, 96.09(4); P17−Pt−Cl, 81.82(4); Cl−Pt−P6, 87.57(4); P36−Pt−C1, 177.80(4); P6−Pt−P17, 165.00(4).

the two Fe atoms on opposite sides. The bond lengths between the Fe and P atoms (2.1774(10) and 2.1802(10) Å) in **6** are longer than the Fe−P2 bond length (2.1342(10) Å) in **4b** but shorter than the Fe−P6 length (2.3075(8) Å) found in **3**. The distances between the C7 atom and the Fe atoms (2.120(4) and 2.129(3) Å) are much longer than the Fe−C3 distance of 1.955(4) Å in **4b**. The Fe−B distances, Fe3−B8 (2.092(4) Å) and Fe2−B11 (2.089(4) Å), are much shorter than those in **4b**, which range from 2.297(4) to 2.636(5) Å.

The reaction of $\mathbf{1a}^-$ with *cis*-dichlorobis(triphenylphosphine)-platinum (II) (eq 5) resulted in the formation of both the η^1-sigma complex, *endo*-6-[*cis*-$(Ph_3P)_2PtCl$]-*exo*-6-(C_6H_5)-*arachno*-6,7-PCB_8H_{11} (**7**) and the η^4-complex, 7-(C_6H_5)-11-$(Ph_3P)_2$-*nido*-11,7,8-$PtPCB_8H_{10}$ (**8**).

$$2\ Na^+[6\text{-}(C_6H_5)\text{-}arachno\text{-}6,7\text{-}PCB_8H_{11}{}^-] + 2\ (PPh_3)_2PtCl_2 \xrightarrow{PS}$$
$$\mathbf{1a}^-$$
$$2\text{-}x\ endo\text{-}6\text{-}[cis\text{-}(Ph_3P)_2PtCl]\text{-}exo\text{-}6\text{-}(C_6H_5)\text{-}arachno\text{-}6,7\text{-}PCB_8H_{11} +$$
$$\mathbf{7}$$
$$x\ 7\text{-}(C_6H_5)\text{-}11\text{-}(Ph_3P)_2\text{-}nido\text{-}11,7,8\text{-}PtPCB_8H_{10} + 2\ NaCl + x\ PSHCl \quad (5)$$
$$\mathbf{8}$$

As depicted in the ORTEP drawing in Figure 9, a crystallographic study verified that the structure of **7** is similar to that of **3**, containing the *cis*-$(Ph_3P)_2PtCl$ unit bonded in the endo orientation at the phosphorus. Consistent with a four-coordinate square-planar configuration, the sum of the bond angles around platinum is 360.09°; however, there is some puckering of the plane, as evidenced by the P36−Pt−C_1 (177.80(4)°) and P6−Pt−P17 (165.00(4)°) bond angles, such that the platinum lies 0.1037(2) Å out of the plane of the four ligand atoms.

The phosphamonocarbaborane intracage distances in **7** are statistically equivalent to those found in **2** and **3**. For example, the P6−B2 length, which might be expected to be most affected by the metal coordination, is again found to be 2.233(5) Å in **7**. Likewise, the C11−P6−B2 bond angles in **3** (87.76(12)°) and **7** (93.4(2)°) are similar. Unlike in **2** and **3**, the platinum does not lie in the P6−B2−B4−B9 plane but is tilted 0.4560-

(22) Callahan, K. P.; Evans, W. J.; Lo, F. Y.; Strouse, C. E.; Hawthorne, M. F. *J. Am. Chem. Soc.* **1975**, *97*, 296−302.
(23) Greene, P. T.; Bryan, R. F. *Inorg. Chem.* **1970**, *9*, 1464−1471.
(24) Grimes, R. N.; Maynard, R. B.; Sinn, E.; Brewer, G. A.; Long, G. J. *J. Am. Chem. Soc.* **1982**, *104*, 5987−5992.

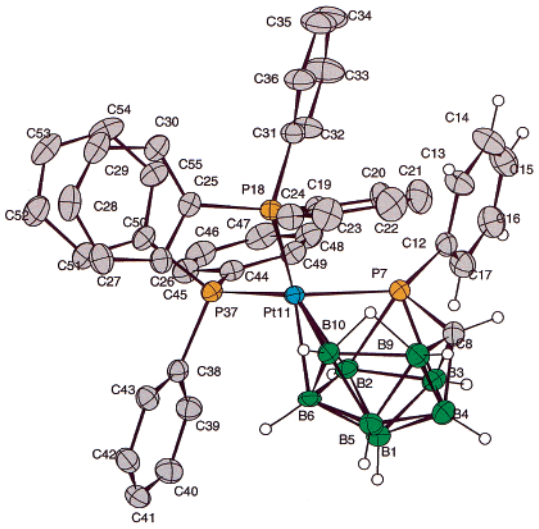

Figure 10. ORTEP representation (30% probability ellipsoids) of 7-(C_6H_5)-11-$(Ph_3P)_2$-*nido*-11,7,8-$PtPCB_8H_{10}$ (**8**). Selected bond lengths (Å) and angles (°): Pt−P18, 2.2788(10); Pt−P37, 2.3274(10); Pt−P7, 2.3267(11); Pt−B2, 2.259(5); Pt−B6, 2.246(4); Pt−B10, 2.277(4); P18−Pt−P37, 102.09(4).

(2) Å out of this plane toward the B8−C7 edge. This is undoubtedly due to the greater steric requirements of the P36-triphenylphosphine compared to its trans chlorine ligand. The Pt−P6 distance (2.3636(12) Å) is similar to that found between the platinum and the phosphorus (P17) of the *trans*-triphenylphosphine (Pt−P17, (2.3782(12) Å). However, both the Pt−P6 and Pt−P17 lengths are longer than the Pt−P36 length (2.2516(12) Å) found for the triphenylphosphine located trans to the chloride, reflecting that chloride is a weaker donor than either triphenylphosphine or the phosphamonocarbaborane. These bond length variations are consistent with the differences found in the Pt−P bonds lengths in *cis*-$(Ph_3P)_2PtCl_2$ (2.251(2) and 2.265(2) Å)[25]and *trans*-$(Ph_3P)_2PtCl_2$ (2.3163(2) Å),[26] where the PPh_3 groups in the two isomers are situated trans and cis, respectively, to a chloride or another triphenylphosphine.

The crystallographically determined structure of 7-(C_6H_5)-11-$(Ph_3P)_2$-*nido*-11,7,8-$PtPCB_8H_{10}$ (**8**) is shown in the ORTEP diagram in Figure 10. In agreement with its predicted 26 skeletal electrons, **8** adopts a normal 11-vertex nido cluster that is derived from an icosahedron by removing one vertex. The five-membered open face has one bridging proton which spans the B9−B10 bond edge. The platinum is thus coordinated in an η^4-fashion to the P7−B2−B6−B10 face of the formal *arachno*-$RPCB_8H_{10}^{2-}$ anion, with the ligand functioning as a 4-electron donor to the platinum. In contrast to **7**, where the P36−Pt−P17 angle between the two triphenylphosphines is 96.09(4)°, in **8** the P18−Pt−P37 angle has increased to 102.09(4)° consistent with the expected change in platinum hybridization upon insertion. However, given the different Pt−P bonding modes in **7** and **8**, it is perhaps surprising that the Pt−P7 bond length (2.3267(11) Å) in **8** is identical to that in **7**. The platinum to B2, B6, and B10 lengths are normal and in the range observed in *nido*-platinatricarbadecaboranyl complexes.[27]

Compound **8** can be envisioned as being formed by a process involving an initial metathesis reaction of $\mathbf{1a}^-$ with *cis*-$(Ph_3P)_2$-$PtCl_2$ to yield an η^1-$(Ph_3P)_2PtCl$- complex such as **7**, followed by a Proton Sponge induced dehydrohalogenation reaction that then results in insertion of the $(Ph_3P)_2Pt$ fragment at the P6−B5−B10−B9 face of the original $\mathbf{1a}^-$ structure. Attempts to thermally convert **7** to **8** were unsuccessful, but inspection of the structure of **7** in Figure 9 reveals that in this complex the chlorine atom is located over the B8−C7 edge of the complex. Thus, dehydrohalogenation with elimination of the chlorine and the nearby B8,9-H hydrogen from **7**, would not produce the structure of **8** in which the platinum is bound to a P−B−B−B face, but would instead produce a complex in which the platinum was bound to a P−B−B−C face. Therefore, it may be that **8** indeed arises by the in situ dehydrohalogenation process above, but that the required intermediate η^1-$(Ph_3P)_2PtCl$- sigma complex may be an isomer of **7** in which the η^1-$(Ph_3P)_2PtCl$- fragment is rotated 180° so that the chlorine is above the B10−B5 edge and in close proximity to the B9,10-H bridging-hydrogen. A dehydrohalogenation from the latter isomer could then lead in a straightforward manner to the structure observed for **8**.

In conclusion, because of their unusual range of readily accessible formal charges (−1 to −3) and coordination geometries (*endo*-η^1, *exo*-η^1, η^4, η^5, or η^6), the 10-vertex phosphamonocarbaborane anions are unique in their abilities to stabilize transition metals in a variety of environments. We are currently investigating the syntheses of an even wider range of phosphamonocarbaboranes and related isoelectronic heteroatomcarbaborane clusters, as well as exploiting the unusual coordinating properties of these clusters to generate new complexes with potential catalytic and bioactivity properties.

Acknowledgment. This paper on "inorganometallic" chemistry is dedicated to Professor Thomas Fehlner on the occasion of his 65th birthday. We thank the National Science Foundation for support of this research. Additional support by the Korea Science and Engineering Foundation is also gratefully acknowledged.

Supporting Information Available: X-ray crystallographic data for structure determinations of **2**, **3**, **4a**, **4b**, **6**, **7,** and **8** (CIF). This material is available free of charge via the Internet at http://pubs.acs.org.

JA020945B

(25) Anderson, G. K.; Clark, H. C.; Davies, J. A.; Ferguson, G.; Parvez, M. *J. Cryst. Spectrosc. Res.* **1982**, *12*, 449−458.
(26) Johansson, M. H.; Otto, S. *Acta Crystallogr.* **2000**, *C56*, e12.
(27) Barnum, B. A.; Carroll, P. J.; Sneddon, L. G. *Organometallics* **1996**, *15*, 645−654.